Formation of Metastable Phases During Mechanical Activation of the Fe–Si Alloy in Liquid Organic Media

S. F. LOMAEVA, E. P. YELSUKOV, A. N. MARATKANOVA, O. N. NEMTSOVA, N. V. IVANOV and A. V. ZAGAYNOV

Physical-Technical Institute, Ural Branch of the Russian Academy of Sciences, Ul. Kirova 132, Izhevsk 426001 (Russia)

E-mail: uds@pti.udm.ru

Abstract

Dispersity, structure, phase composition and magnetic properties of the powder obtained by grinding the alloy of iron with silicon (with the atomic concentration of Si equal to 20 %) in liquid hydrocarbons (heptane, heptane with oleic acid as an additive) in a ball planetary mill were investigated by means of X-ray structural analysis, Mössbauer and Auger spectroscopy, secondary ion mass spectrometry, magnetic measurements. It was shown that during grinding the alloys get saturated with the products of destruction of the organic liquid (C, O, H) with the formation of metastable amorphous and carbide phases. With an increase in grinding time, the particle size decreases to 0.1–0.2 μm. Isochronous (500 °C, 1 h) annealing leads to the crystallization of the amorphous phase with the formation of ferric silicocarbide Fe_8Si_2C, Fe_3Si and C in the case of grinding in heptane, and Fe_3C with SiO_2 in the case of grinding with oleic acid added. The magnetic characteristics of the powder depend on the time and medium of grinding, and also on annealing temperature. An increase in coercivity from 10 to 180 A/cm correlates with the amount of the formed silicocarbide. The resulting silicocarbide has the composition Fe_8Si_2C; it has a triclinic lattice with the parameters: $a = 6.401$ Å, $b = 6.434$ Å, $c = 9.884$ Å, $\alpha = 83.590°$, $\beta = 99.343°$, $\gamma = 120.924°$; it is a ferromagnetic with Curie temperature T_C equal to 788 K, stable up to 870 K.

INTRODUCTION

Alloys Fe–Si–C attract much attention because they play an important part in the processes involved in the production of steel and cast iron [1–15]. Amorphous alloys Fe–C–Si are attractive since their mechanical strength, plasticity, corrosion stability and magnetic properties exceed the characteristics of technical-grade cast iron substantially.

Various metastable phases Fe–Si–C obtained either by rapid cooling from the melts or by means of mechanical grinding were investigated. The existence of various metastable phases was reported, for example amorphous phases [3], *bcc* [8], orthorhombic [6, 7, 10], triclinic [2, 13], hexagonal [1, 11], cubic with α- and β-Mn structural type [8]. It was assumed that ferric silicocarbide exists, but the mechanism of formation and the nature of these structural constituents have not been revealed completely yet. There is also no distinctness about the chemical composition of this compound: its formula is represented in different manners in literature – Fe_3SiC, Fe_4SiC, $Fe_{10}Si_2C_2$ [12], $Fe_{10}Si_2C_3$ [1], Fe_8Si_2C [2], Fe_9SiC_2 [11].

Grinding of metals and alloys in liquid organic media is used for rapid decrease in particle size and for obtaining more uniform particle size distribution, and also for controlling structural, phase and morphological, as well as thermal and magnetic properties of the resulting powders [16, 17].

For the first time, in [18–23] we investigated the sequence of structural and phase transformations occurring when iron is ground in heptane medium, including the case when a surface-active substance (SAS) was present, and the effect of SAS on dispersity, particle shape, magnetic characteristics and the kinetics of structural and phase transformations. It was shown that at the initial stage of grinding the powder acquire nanocrystalline structure. Further grinding results in the saturation of the boundaries of iron particles with the products of destruction of the grinding medium –

C, O, H, Si – which results in the formation of supersaturated solid insertion solutions, amorphous-like and disordered phases; at the final stages carbide and oxide phases are formed.

Grinding of Fe–So alloy in organic liquid (toluene) was carried out for the first time by the authors of [24]; they showed that at the final stage of grinding (32 h) saturation with carbon results in the formation of the amorphous alloy $Fe_{70}Si_{12}C_{18}$ with Curie temperature T_C equal to 500 K. It was reported in [2, 9] that amorphous alloys Fe–Si–C are formed during quenching from the melt if the atomic concentration of a metalloid in the alloy exceeds 30 %, silicon is present at a level not less than 5 %, while carbon concentration is above 10 %.

The goal of the present work was to investigate the processes of formation of metastable phases during grinding $Fe_{80}Si_{20}$ alloy in the liquid organic medium (heptane), the effects of thermal treatment on structural, phase and magnetic characteristics of the resulting phases, and the effect of SAS additive (oleic acid) on the dispersity, structure, phase composition and magnetic characteristics of powders.

EXPERIMENTAL

The initial material was the powder of Fe–Si alloy (with the atomic concentration of Si 20 %) with particle size ≤300 μm. Grinding was carried out in a ball planetary mill Pulverisette-7 with the vessel 45 cm^3 in volume and with 16 gridning balls 12 mm in diameter; the balls were made of ShKh15 steel containing 1 % C and 1.5 % Cr. For each given grinding time t_{gr}, tight vessel was charged with 10 g of the initial iron powder together with the milling balls. The rest space of the vessel was filled with heptane or the solution containing SAS – oleic acid (OA) in heptane, with the mass concentration of 0.3 %. Grinding time was varied within the range 1 to 99 h. In order to avoid a decrease in SAS concentration, SAS solution was replaced with the fresh one every 3 h during treatment. Temperature in the vessel during grinding was 60–80 °C. An increase in the sample mass due to wear of the vessel and balls was discovered only for grinding in argon (5 %). To obtain a reference sample of the ordered Fe–Si alloy (with the mass concentration of Si 20 %), the powder was ground in for 12 h in argon medium and subjected to vacuum (10^{-3} Pa) annealing according to the scheme: heating to 800 °C, exposure for 1 h, cooling to 500 °C, exposure for 4 h, cooling to room temperature.

The image of powder in secondary electrons and chemical composition of the surface layers were obtained using JAMP-10S Auger spectrometer.

Investigation of the shape and size of separate particles of the powder was carried out in the air in the regime of topography measurement by means of atomic force microscopy (AFM) with the scanning probe microscope P4-SPM-MDT of HT-MDT company. Silicon cantilevers of Silicon-MDT company with the needle curvature radius less than 10 nm and the needle convergence angle at the vertex less than 20°. The functions of particle size distribution were obtained with the laser diffraction microanalyzer Analyzette-22.

The X-ray structural investigation was carried out with DRON-3M diffractometer using CuK_α radiation. The grain size and lattice microdistortion values were calculated from the line broadening values by means of harmonic analysis [25]. Mossbauer investigation was performed with YaGRS-4M spectrometer operating in the regime of constant acceleration with ^{57}Co in Cr matrix as a source of γ radiation. The distribution functions for superfine magnetic fields $P(H)$ were determined from the spectra with the help of the generalized regular algorithm [26].

Analysis of the powder for hydrogen content was carried out by means of secondary ion mass spectrometry (SIMS) with MS-7201M mass spectrometer. X-ray photoelectron spectroscopy (XPES) was carried out with ES-2401 spectrometer using MgK_α radiation, vacuum in the chamber of the spectrometer was 10^{-5} Pa, the accuracy of line position measurement was 0.2 eV. Decomposition of the spectra into the components was carried out using the procedure described in [27]. The relative error of measurements of the line intensity was about 10 %. All the above-indicated measurements were carried out at room temperature. The data on specific magnetization of saturation s and coercivity H_c were obtained

with a vibration magnetometer with the maximal external constant magnetic field H_{ext} = 12 kOe at room temperature. Thermomagnetic measurements were carried out within temperature range 300–1100 K using the set-up for measuring the dynamic magnetic susceptibility with the amplitude of variable magnetic field 1.25 Oe and frequency 120 Hz in a quartz ampoule filled with argon; linear heating and cooling rate was 60 deg/min.

RESULTS AND DISCUSSION

In the initial state, the powder of $Fe_{80}Si_{20}$ alloy had saturation magnetization σ = 150 A m^2/kg, coercivity H_c = 10 A/cm, lattice parameter of the ordered alloy $Fe_{80}Si_{20}$ a = 0.2838 nm, Curie temperature T_C = 865 K, mean grain size $<L>$ = 100 nm.

According to the data of atomic force microscopy (Fig. 1), powder samples obtained in heptane (H) and in heptane with a surface-active substance added (H_{OA}) after grinding for maximal time (t_{gr} = 99 h) are composed of the particles 0.1–0.2 μm in size, with a shape close to ellipsoid. Dispersity of Fe–Si powder is about an order of magnitude higher than that of Fe powder obtained under the same conditions [20]. The image of powder samples in secondary electrons (Fig. 2) shows that powder H consists of stone-like agglomerates, H_{OC} powder is less agglomerated. The curves of size distribution for t_{gr} = 99 h (Fig. 3) have several maxima, due to the fact that the particles form agglomerates differing in size. Mean size of agglomerates for H is 22 μm, for H_{OA} 2 μm. Unlike the systems based on Fe for which the presence of oleic acid caused a decrease in the size of particles themselves [20], for Fe–Si systems sim-

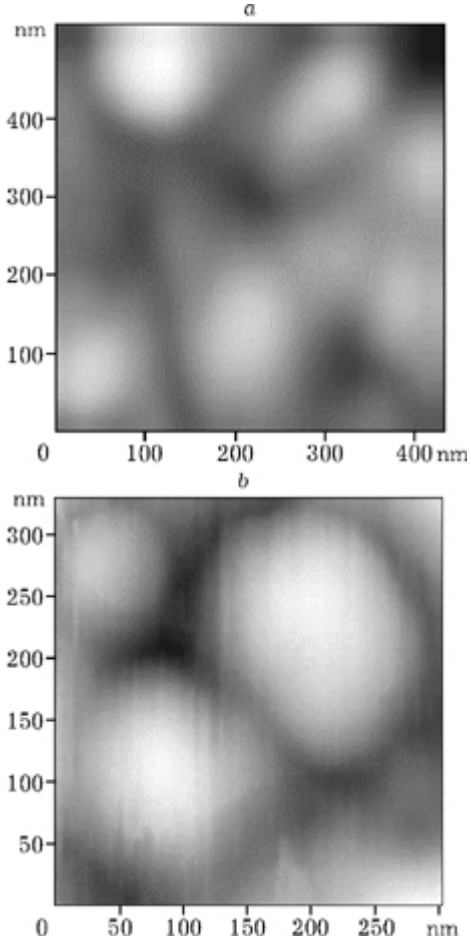

Fig. 1. AFM image of the particles of $Fe_{80}Si_{20}$ alloy powder after 99 h grinding: *a* – in heptane (H powder), *b* – in SAS solution (H_{OA} powder).

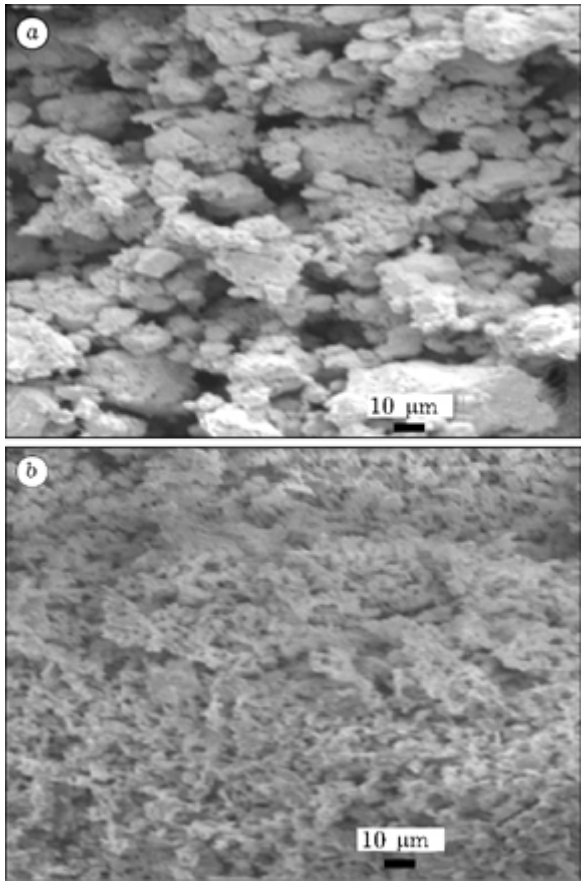

Fig. 2. The secondary electron images of the alloy powder particles after 99 h grinding: *a* – in heptane, *b* – in SAS solution.

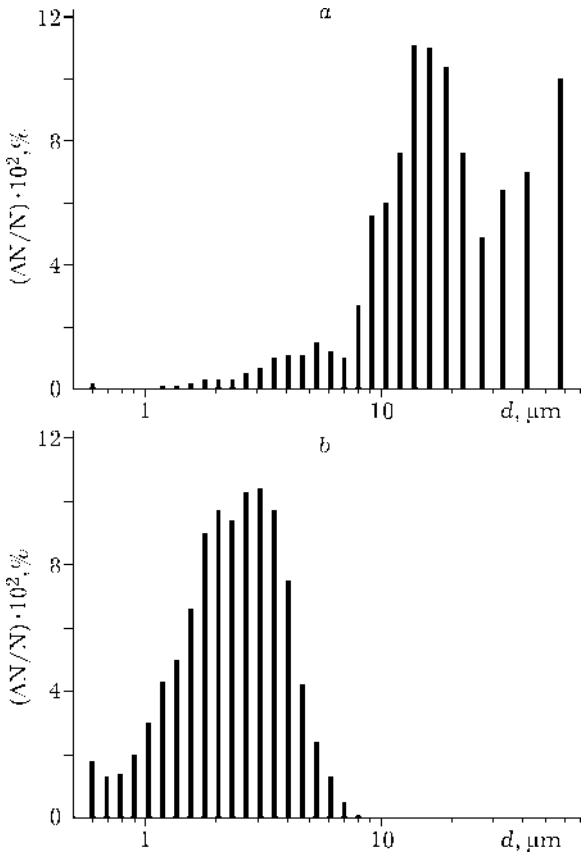

Fig. 3. The Size distribution of alloy powder particles after 99 h grinding: *a* – in heptane, *b* – in SAS solution.

ilar additives have only a slight effect on particle size but cause a substantial decrease in the size of the agglomerates of particles.

According to the data of Auger spectroscopy (Fig. 4), similarly to the data obtained by XPES, the powder does not contain any foreign impurities; it contains only iron, silicon, carbon. Analysis for hydrogen content by means of SIMS showed that atomic hydrogen is present

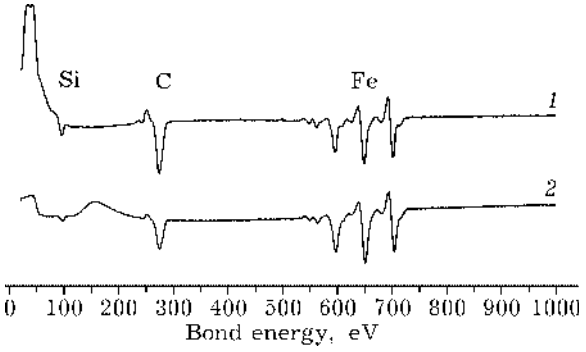

Fig. 4. Auger spectra of the alloy powder after 99 h grinding: *1* – in heptane, *2* – in SAS solution. Analysis was carried out after removing the surface layer 10 nm thick.

in equal amounts both in the initial powder samples and in those annealed at 500 °C.

The diffraction patterns of powder ground for different time intervals are shown in Fig. 5, *a*, *c*. For t_{gr} = 1–12 h, diffraction patterns are not shown because the changes in them are similar: broadening of the lines related to the bcc phase is observed, which is more substantial for H powder samples. After t_{gr} = 24 h, a halo appears at the base of ((200) line (see Fig. 5, *a*, *b*, curves *2*), which is due to the formation of the amorphous phase (AP) Fe–Si–C; its amount in H powder increases with an increase in t_{gr}. In the H_{OC} powder, along with a small amount of the AF, the reflections of a new phase appear for t_{gr} equal to 48 and 99 h (see Fig. 5, *c*, curves *3* and *4*).

The size of grains, microdistortions and the parameter of *bcc* lattice of the $Fe_{80}Si_{20}$ alloy were determined on the basis of broadening of the X-ray lines for t_{gr} = 1–24 h (Table 1). We failed to carry out the analysis for large t_{gr} values because of strong line broadening and overlap. As early as after 1 h grinding, the powder becomes nanocrystalline; further grinding results in the grain size decreased to 30–40 Å. The lattice parameter and micro-distortions in powder H increase with an increase in t_{gr} due to saturation with carbon and accumulation of the AP. For H_{OA} powder, the lattice parameter remains unchanged, while microdistortions decrease, which is connected with the effect of the surfactant. First, the particles are subjected to stronger plastic deformation during grinding [28], which can cause crystallization of the AP and elimination of microdistortions. Second, SAS decreases the surface energy thus simplifying insertion of admixture atoms into the alloy lattice. in addition, the particle volume get saturated not only with carbon but also with oxygen; the latter decreases solubility of carbon [29] and therefore promotes precipitation of the carbide phases. An evidence of more rapid saturation of the alloy with non-magnetic admixtures during grinding in SAS solution is a sharper decrease in the saturation magnetization (Table 2). An increase in coercivity with an increase in t_{gr} during grinding in SAS (see Table 2) and almost constant coercivity during grinding in heptane are also evidences of precipitation of carbide phases in H_{OA} powder.

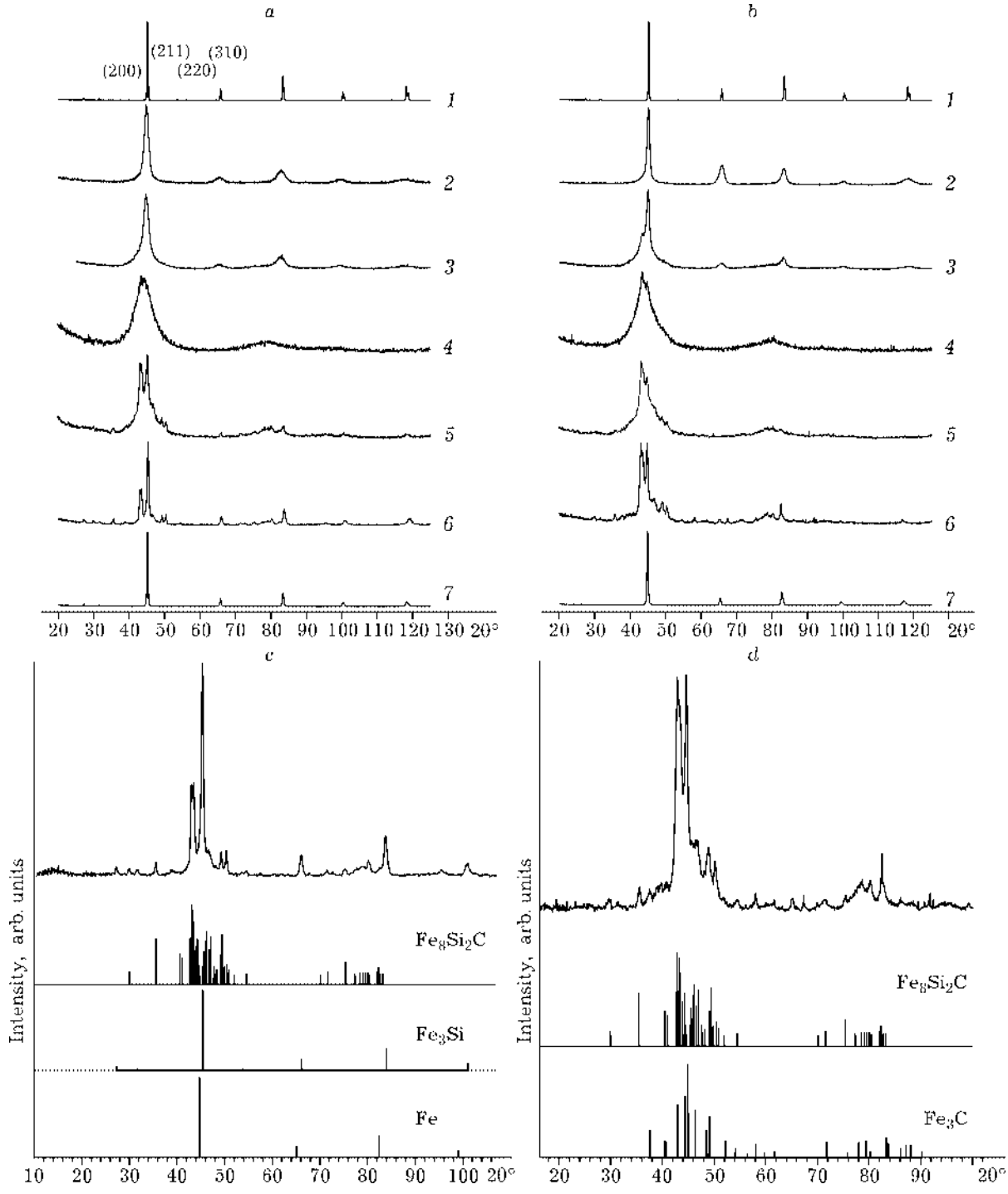

Fig. 5. Diffraction patterns of the allow powder ground: *a* – in heptane, *b* – in SAS solution, *c* – in heptane after annealing at 500 °C, *d* – in SAS solution after annealing at 500 °C; *1* – the refernce alloy $Fe_{80}Si_{20}$, *2–4* – for t_{gr} equal to 24, 48, 99 h, respectively; *5–7* – for t_{gr} = 99 h, after annealing at 400, 500 and 800 °C, respectively.

Annealing of powder samples at a temperature of 400 °C results in partial crystallization of the AP; it gets completely crystallized at 500 °C. The results of the analysis of the formed phases are shown below. Judging from the lattice parameter, H powder after annealing at 800 °C returns into the state corresponding to $Fe_{80}Si_{20}$ alloy. For H_{OA}, an increase in the lattice parameter is observed, corresponding to $Fe_{87}Si_{13}$ [30] which is depleted in silicon in comparison with the initial alloy. Depletion is caused by the formation of SiO_2 in the particle

TABLE 1

Changes in grian size <*L*>, microdistortion c and lattice parameter a of the *bcc* alloy $Fe_{80}Si_{120}$ depending on time of grinding t_{gr} in different media

Parameter	t_{gr}, h				
	1	3	6	12	24
		In heptane			
<*L*>, ± 5, Å	51	42	35	40	30
ε, ± 0.03 %	0.3	0.39	0.42	0.5	0.45
a, ± 0.003, Å	2.841	2.845	2.848	2.848	2.850
*a**, ± 0.003, Å	2.836	2.855			
		In SAS solution			
<*L*>, ± 5, Å	77	52	59	42	40
ε, ± 0.03 %	0.31	0.30	0.36	0.28	0.23
a, ± 0.003, Å	2.843	2.844	2.843	2.843	2.843

*After annealing at 800 °C (t_{gr} = 99 h).

TABLE 2

Changes in saturation magnetization σ and coercivity H_c depending on grinding time t_{gr} and annealing temperature T_{ann} in different media

Parameter	t_{gr}, h			T_{ann}, °C (t_{gr} = 99 h)		
	24	48	99	400	500	800
		In heptane				
σ, A m^2/kg	150	150	133	139	146	148
H_c, A/cm	18	19	21	87	180	10
		In SAS solution				
σ, A m^2/kg	137	139	121	126	129	157*
H_c, A/cm	22	31	45	83	155	83

*For $Fe_{87}Si_{13}$ alloy, σ ~ 200 A m^2/kg [30].

volume due to the oxygen of oleic acid decomposing during grinding. The presence of nonmagnetic inclusions in the alloy is also evidenced by the fact that magnetization of H_{OA} powder after annealing at 800 °C is much lower (see Table 2) than the value characteristic of the $Fe_{87}Si_{13}$ alloy [31].

The diffraction patterns of the powder samples after annealing at 500 °C are shown in Fig. 5, *c*, *d*. The phase and structural analysis carried out using database [32] showed that the new phase is ferric silicocarbide (SC) Fe_8Si_2C with the triclinic lattice, space group *P*1 with 32 atoms in a unit cell and the atomic density of 0.0920 at./Å^3. The lattice parameters of SC obtainedin different media slightly differ from each other, which is connected with the effect of oxygen formed in the alloy as a result of SAS destruction. It is known [33] that oxygen can substitute some carbon atoms in ferric carbides thus forming complicated intercalation compounds, that is, oxycarbides. In the case under our consideration, the formation of silico-oxycarbide is possible [1].

An image of the lattice of silicocarbide Fe_8Si_2C composed with the help of the programme described in [34] is shown in Fig. 6. Mechanical grinding of the dry mixture

TABLE 3

Lattice parameters and angles for ferric oxycarbide Fe_8Si_2C synthesized in different media

Grinding medium	Lattice parameters, Å			Lattice angles, deg		
	a	*b*	*c*	α	β	γ
Heptane	6.413	6.449	9.724	83.651	99.307	120.423
SAS solution	6.449	6.469	9.711	83.550	99.500	120.900

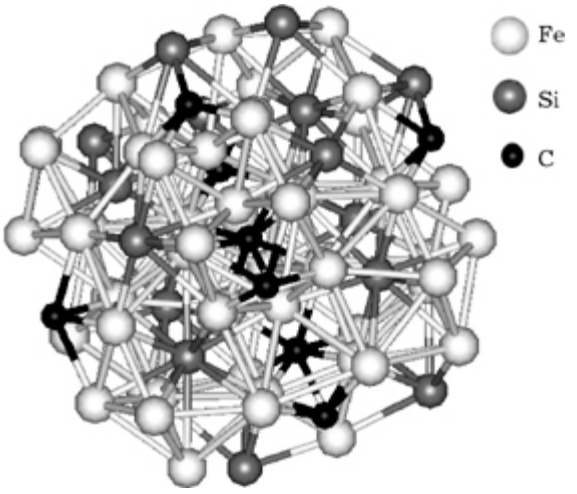

Fig. 6. Image of the crystal structure of ferric silicocarbide Fe_8Si_2C.

70 % Fe + 13 % Si + 17 % C (carbon in the form of graphite) followed by crystallization of the resulting AP leads to the formation of silicocarbide Fe_5SiC with orthorhombic lattice [35]. The formation of a compound with lower lattice symmetry occurring in the liquid organic media may be due to the presence of hydrogen in the grinding medium. It is known [36] that hydrogen may get built into the structure of carbides changing their characteristics, for example increasing thermal stability of cementite [22].

In addition to ferric SC, the Fe_2Si phase is formed in H powder, Fe_3C and α-Fe in H_{OA} (Table 4). The analysis of structural and phase transformations occurring in the alloy during grinding and annealing allows one to conclude that the first product of AP decomposition is SC of quite definite composition, and after it other phases are formed. With an excess of Si in the alloy (in the case of powder H), Fe_3Si is formed; with a lack of Si and an excess of Fe and C (in the case of H_{OA} powder) Fe_3C is formed.

TABLE 4

Results of phase analysis of the powder after 99 h of grinding in different media and annealing at 500 °C

Grinding	Content, vol. %			
medium	Fe_8Si_2C	Fe_3Si*	Fe_3C	α-Fe
Heptane	65	35	0	0
SAS solution	75	0	20	5

*Type DO_3.

The reflections of graphite are absent in the diffraction patterns of powder samples after annealing at 800 °C; this may be connected with the formation of fine graphite particles built into a ferrite matrix [37] or amorphous films on the particle surface [38]. In order to reveal the state in which carbon is present after annealing of the powder samples, we analysed the surface by means of XPES (Fig. 7). The quantitative analysis showed that the layer under investigation (about 100 E deep as analysed by XPES [39]) contains a substantial amount of carbon (Table 5). In C1*s* spectra, the line with E_b ~ 282.5 eV corresponds to ferric carbides, E_b ~ 284.0 eV to graphite, E_b = 285.0 eV to the carbon of C–H groups, E_b > 286.0 eV to the carbon of oxygen-containing organic groups [39, 40]. The C1*s* spectra of both powder samples after annealing at 500 °C contain the lines related to carbides (E_b ~ 282.5 eV); their

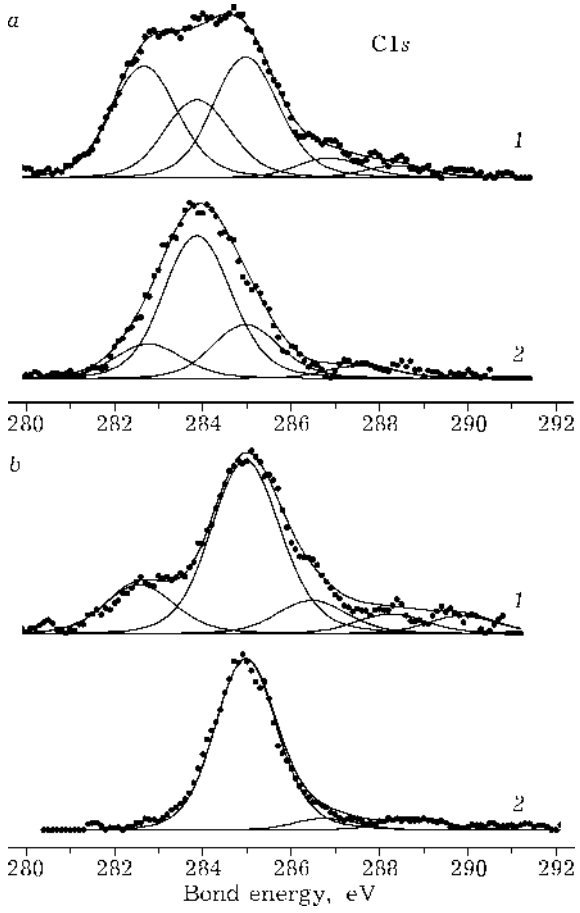

Fig. 7. XPES of the alloy powder after 99 h grinding: *a* – in heptane, *b* – in SAS solution; *1*, *2* – annealing at 500 and 800 °C, respectively.

TABLE 5

Changes in the composition of the surface layers of powder samples ground in different media for 99 h, depending on annealing temperature, at. %

Grinding medium	C				O				Fe				Si			
	At a temperature of, °C															
	Initial	400	500	800	Initial	400	500	800	Initial	400	500	800	Initial	400	500	800
Heptane	49	58	61	56	37	30	27	31	10	4	2	0	4	8	10	13
SAS solution	47	52	52	73	39	33	38	21	7	5	4	0	7	10	6	5

contribution almost disappears after annealing at 800 °C. Carbon is present on the surface of H powder as a thin graphite film (E_b = 284.0 eV), while on the surface of H_{OA} powder it is present as amorphous carbon (E_b = 285.0 eV).

The forward traces of thermal dependencies of the magnetic susceptibility of initial powder ground for 99 h exhibit several fractures (Fig. 8, *a*, *c*). The first fracture at T_C equal to 620 and 600 K for H and H_{OA} powder samples, respectively, reveals the Curie temperature of the AP, which is in good agreement with the published literature data [41, 42]. Lower T_C for H_{OA} powder is an evidence of higher metalloid content of this alloy. The second fracture at T_C = 760–780 K reveals the Curie temperature of SC. Since the fraction of the AP is much higher in H powder, a stronger jump is observed in the temperature dependence of magnetic susceptibility for H powder (see Fig. 8, *a*) at about 900 K, when crystallization of the AP and decomposition of SC occur. Only one inflection is observed on the back trace. For H

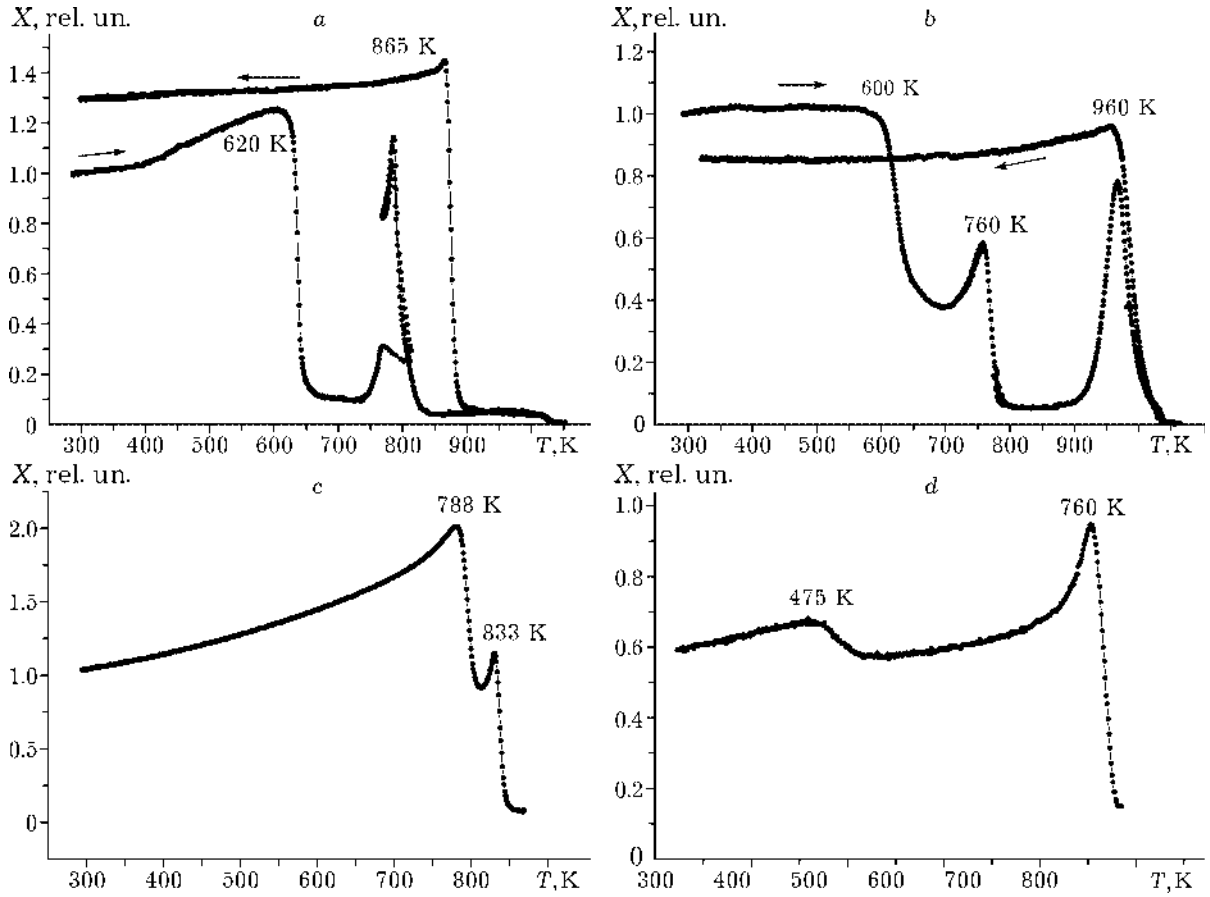

Fig. 8. Temperature dependencies of the dynamic magnetic susceptibility of alloy powder after 99 h grinding: *a* – in heptane, *b* – in SAS solution, *c* – in heptane after annealing at 500 °C, *d* – in SAS solution after annealing at 500 °C. Heating and cooling are indicated with arrows along the curves.

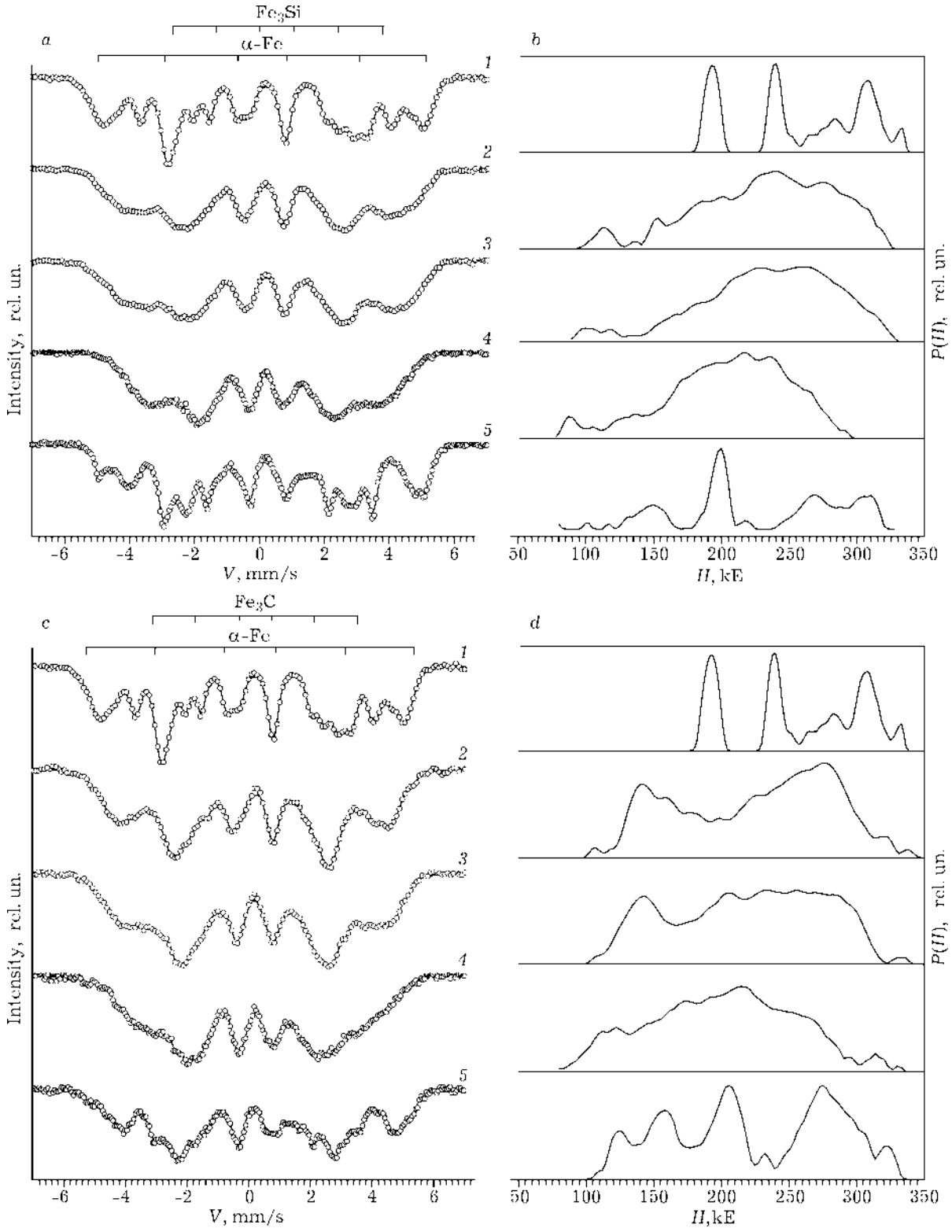

Fig. 9. Mössbauer spectra of the powder ground in heptane (*a*) and in SAS solution (*b*): *1* – reference alloy $Fe_{80}Si_{20}$, *2–4* – for t_{gr} equal to 24, 48, 99 h, respectively, *5* – for t_{gr} equal to 99 h, after annealing at 500 °C.

powder, the observed T_C equal to 865 K is characteristic of $Fe_{80}Si_{20}$ alloy; this means that the alloy returns to its initial state. For H_{OA} powder, Curie temperature increases substantially and becomes equal to 960 K, which corresponds to the alloy with silicon content of 13–14 %

[30] and agrees with the data of X-ray structural analysis.

Two inflections are observed in the temperature curves of magnetic susceptibility of powder samples after annealing at 500 °C (see Fig. 8, *b, d*). For H powder, T_C = 475 K, which coincides with the known Curie temperature for Fe_3C; T_C equal to 760 K relates to the SC phase. We explain a decrease in T_C for the SC phase formed during grinding in SAS solution by the presence of oxygen in SC. So, the results of phase analysis carried out on the basis of temperature curves of magnetic susceptibility are in good agreement with the data obtained by X-ray structural analysis.

Mössbauer spectra and the distribution functions of superfine magnetic fields $P(H)$ are shown in Fig. 9. A broad distribution of $P(H)$ is observed for grinding in heptane. With an increase in t_{gr}, the $P(H)$ function shifts to the region with smaller superfine magnetic field values, which characterized the process of amorphous phase formation in the Fe–Si alloy saturated with carbon [24]. The addition of SAS into the grinding medium changes the situation: the $P(H)$ function becomes bimodal; the intensity increases substantially within the range 100–150 kOe; this is an evidence of layering processes in the alloy for $t_{gr} > 24$ h.

The results of discrete treatment of Mössbauer spectra of powder samples after annealing at 500 °C are shown in Table 6. The results of phase analysis on the basis of Mössbauer spectra are in qualitative and quantitative agreement with the results of X-ray structural analysis. In the case of H powder, we succeeded in describing the spectrum with four sextets corresponding to four versions of Fe surrounding by Si and C atoms (see Fig. 6). In the case of H_{OA} powder, the number of sextets increased to six; this may be due to the presence of oxygen atoms in the nearest surroundings of Fe. The values of the mean field at the nucleus correspond for SC synthesized in different media.

On the basis of investigation carried out in the present work, we may suggest a scheme of phase transformations that occur during grinding Fe–Si alloy in liquid organic media followed by thermal treatment procedures (Fig. 10).

TABLE 6

The parameters of Mössbauer spectra of Fe–Si alloy powder after annealing at 500 °C

Gridning medium	Phase	Superfine field H, T ± 0.3	Measured shift d, mm/s ± 0.02	Area of spectrum, relative % ± 3
Heptane	Fe_3Si [43]	31.0	0.08	15
		20.0	0.25	34
	Fe_8Si_2C	30.9	0.30	8
		27.6	0.32	15
		25.8	0.32	12
		14.5	0.12	16
		H_m = 23.5		
SAS solution	α-Fe [44]	32.4	0.11	7
	Fe_3C [44]	20.5	0.21	23
	Fe_8Si_2C	30.4	0.23	8
		28.6	0.29	11
		26.9	0.31	18
		24.6	0.19	5
		15.9	0.13	19
		12.7	0.08	9
		H_m = 22.8		

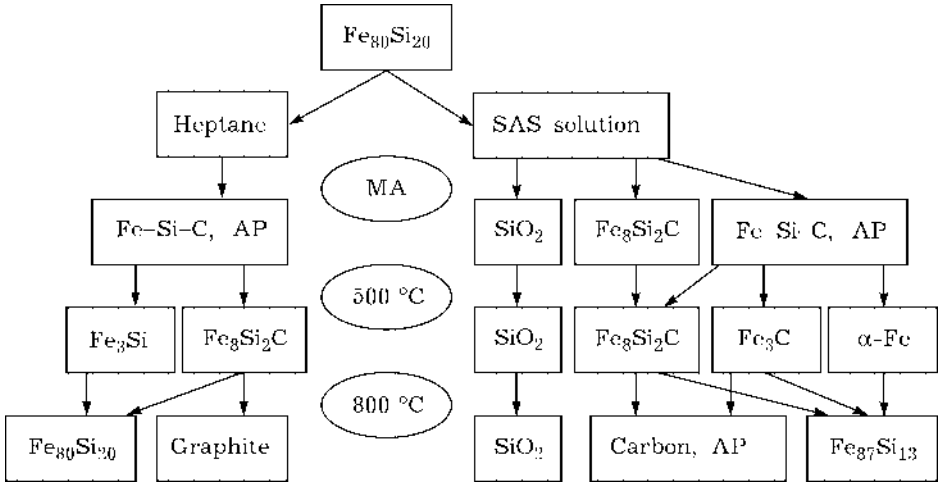

Fig. 10. Scheme of phase transformations of the Fe–Si alloy during grinding followed by annealing.

CONCLUSIONS

Investigation of dispersity, particle shape, formation of the structural and phase composition and magnetic characteristics during grinding $Fe_{80}Si_{20}$ alloy in heptane and with SAS (oleic acid) added showed that the presence of silicon allows one to increase the dispersity of particles to 0.1–0.2 μm, while SAS strongly decreases agglomeration of the resulting powder. A sequence of structural and phase transformations during grinding Fe–Si alloy in liquid organic media was established: the formation of nanocrystalline structure, saturation of the particle volume with the products of destruction of the grinding medium (C, O, H) with the formation of solid solutions and amorphous phases; formation of chemical compounds: silicocarbides, ferric carbides, *etc.*

An increase in coercivity of the resulting powder samples from 10 to 180 A/cm correlates with the amount of silicocarbide formed.

Silicocarbide Fe_8Si_2C synthesized during grinding in heptane has a triclinic lattice with parameters: $a = 6.413$ Å, $b = 6.449$ Å, $c = 9.724$ Å, $\alpha = 83.651^o$, $\beta = 99.307^o$, $\gamma = 120.423^o$; it is a ferromagnetic with Curie temperature equal to 788 K, mean superfine field at the nucleus H equal to 23.5 T, stability up to the temperature of 870 K. If a source of oxygen (oleic acid) is present in the grinding medium, a part of carbon atoms in silicocarbide is replaced by oxygen, which results in a definite change in lattice parameters, Curie temperature and the characteristics of local atomic surroundings.

Acknowledgements

The authors thank G. N. Konygin, A. I. Ulyanov, N. B. Arsentyeva, F. Z. Gilmutdinov for assistance in carrying out measurements.

The work has been supported by RFBR (Proejct No. 04-03-96023).

A. N. Maratkanova thanks the Russian Foundation for Promotion of Science for financial support.

REFERENCES

1 H. J. Goldshmidt, Splavy vnedreniya, Mir, Moscow, 1971.
2 J. Lacaze, B. Sundman, *Metall. Mater. Trans. A*, 22A (1991) 2211.
3 A. Inoue, S. Furukawa, T. Masumoto, *Ibid.*, 18 (1987)715.
4 Ya. N. Malinochka, V. Z. Dolinskaya, *Liteynoye Proizvodstvo,* 7 (1970) 26.
5 Ya. N. Malinochka, V. Z. Dolinskaya, *Struktura i Svoystva Chuguna i Stali*, 26 (1967) 23.
6 N. D. Edneral, V. A. Lyakishev, Yu. A. Skakov, *FMM*, 43, 3 (1977) 426.
7 G. Konoval, L. Zwell, L. A. Gorman *et al.*, *Nature*, 164 (1959) 56.
8 Y. C. Chen, C. M. Chen, K. S. Su, *Mater. Sci. Eng. A*, 133 (1991) 596.
9 T. Tanaka, S. Nasu, K. Nakagawa *et al.*, *Mater. Sci. For.*, 88–90 (1992) 269.
10 J. M. Dubouis, G. Le Caër, *Acta Met.*, 25 (1977) 609.
11 V. F. Bashev, *FMM*, 55, 2 (1983) 331.
12 L. A. Solntsev, V. D. Shifrin, O. N. Miroshnichenko *et al.*, *Metally*, 4 (1993) 102.
13 P. P. Spinat, C. Brouty, A. Whuler *et. al.*, *Acta Crystallogr.*, B31 (1975) 541.
14 I. Schmidt, E. Hornbogen, *Iron-Carbon Glasses*, 69, 4 (1978) 221.
15 R. Ruhl, M. Cohen, Trans. Met. Soc. AIME, 1969, vol. 245, pp. 241–251.

16 P. A. Rebinder, Poverkhnostnye yavleniya v dispersnykh sistemakh. Fiziko-khimicheskaya mekhanika, Nauka, Moscow, 1979.
17 L. S. Vasile'v, S. F. Lomaeva, *Chem. Sustain. Develop.*, 10 1–2 (2002) 203.
http://www-psb.ad-sbras.nsc.ru
18 S. F. Lomayeva, E. P. Yelsukov, G. N. Konygin *et al.*, *Colloids Surf.*, A 162, 1–3 (1999) 279.
19 L. S. Vasile'v, S. F. Lomaeva, *Metally*, 4 (2003) 48.
20 S. F. Lomaeva, E. P. Yelsukov, G. N. Konygin, *Kolloid. Zh.*, 62 (2000) 644.
21 E. P. Yelsukov, S. F. Lomayeva, G. N. Konygin *et al.*, *Nanostruct. Mater.*, 12 (1999) 483.
22 L. S. Vasil'ev, S. F. Lomayeva, *J. Mater. Sci.*, 39 (2004).
23 S. F. Lomaeva, N. V. Ivanov, E. P. Yelsukov, *Kolloid. Zh.*, 66, 2 (2004) 216.
24 G. N. Konygin, E. P. Yelsukov, V. A. Barinov, in I. Ortalli (Ed.), Proc. of the Int. Conf. on the Applications of the Mössbauer Effect (ICAME'95), Rimini, Italy, Sept. 10–16, 1995, S.I.F., Bologna, 1996, p. 157.
25 B. E. Warren, J. Averbach, *J. Appl. Phys.*, 21, 6 (1950) 595.
26 E. V. Voronina, N. V. Ershov, A. L. Ageev, Yu. A. Babanov, *Phys. Stat. Sol.* (*b*), 160 (1990) 625.
27 V. I. Povstugar, A. A. Shakov, S. S. Mikhaylova *et al.*, *Zh. Anal. Khim.*, 53, 8 (1998) 795.
28 V. V. Likhtman, E. D. Shchukin, P. A. Rebinder, Fiziko-khimicheskaya mekhanika metallov, Izd-vo AN SSSR, Moscow, 1962.
29 O. Kubashevskiy, Diagrammy sostoyaniy dvoynykh sistem na osnove zheleza, Metallurgiya, Moscow, 1985.
30 E. P. Yelsukov, V. A. Barinov, G. N. Konygin, *Metallofizika*, 11, 4 (1989) 52.
31 E. P. Elsukov, G. N. Konygin, V. A. Barinov, E. V. Voronina, *J. Phys.: Condens. Matter*, 4 (1992) 7597.
32 Powder Diffraction File, Alphabetical Index, Inorganic Phases, International Center for Diffraction Data, Pensylvania, 1985.
33 A. P. Gulyaev, Metallovedeniye, Metallurgiya, Moscow, 1978.
34 B. Ravel, Program ATOMS version 2.46b, University of Washington, 1996.
35 S. F. Lomaeva, E. P. Yelsukov, A. N. Maratkanova *et al.*, *Pis'ma v ZhTF*, 30, 18 (2004) 46.
36 V. I. Shapovalov, Vliyaniye vodoroda na strukturu i svoystva zhelezo-uglerodistykh splavov, Metallurgiya, Moscow, 1982.
37 Y. C. Chen, C. M. Chen, K. C. Su, *Mater. Sci. Eng.*, A133 (1991) 596.
38 B. Bokhonov, M. Korchagin, *J. Alloys Comp.*, 333 (2002) 308.
39 V. I. Nafadov, Rentgenoelektronnaya spektroskopiya khimicheskikh soyedineniy, Khimiya, Moscow, 1984.
40 G. Beamson, D. Briggs, High Resolution XPS of Organic Polymer: the Scienta ESCA300 Database, Chichester, Wiley, 1992.
41 G. P. Huffman, P. R. Errington, P. M. Fisher, *Phys. Stat. Sol.*, 22 (1967) 473.
42 Yu. V. Maksimov, I. P. Suzdalev, R. A. Arents, *FTT*, 14 (1972) 3344.
43 M. B. Stearns, *Phys. Rev.*, 129 (1963) 1136.
44 V. G. Gavrilyuk, Raspredeleniye ugleroda v stali, Nauk. Dumka, Kiev, 1987.